Eur Biophys J (2004) 33: 396–411
DOI 10.1007/s00249-003-0374-z

ARTICLE

Dietrich Gradmann · Carl M. Boyd

Current–voltage–time records of ion translocating enzymes

Received: 9 October 2003 / Accepted: 11 November 2003 / Published online: 5 February 2004

Abstract Membrane currents, as non-linear functions of membrane voltage, V, and time, t, can be recorded quickly by triangular V protocols. From the differences, $dI(V,t)$, of these relationships upon addition of a putative substrate of a charge-translocating membrane protein, the $I(V,t)$ relationships of the transporter itself can be determined. These relationships likely comprise a steady-state component, $I_a(V)$, of the active transporter, and a dynamic component, $p_a(V,t)$, of its V- and time-dependent activity, p_a. Here, the steady-state component is modeled by a central reaction cycle, which senses a fraction δ_{tr} of the total V, whereas $1-\delta_{tr}$ can be assigned to an inner and outer pore section with δ_i and δ_o, respectively ($\delta_i+\delta_{tr}+\delta_o = 1$). For the enzymatic cycle, fast binding/debinding is assumed, plus V-sensitive and -insensitive reaction steps which may become rate limiting for charge translocation. At given substrate concentrations, $I_a(V)$ is defined by eight independent system parameters, including a coefficient for the barrier shape of charge translocation. In ordinary cases, the behavior of $p_a(V,t)$ can be described by two rate constants (for activation and inactivation) and their respective V-sensitivity coefficients. Here, the effects of the individual system parameters on $I(V,t)$ from triangular V-clamp experiments are investigated systematically. The results are illustrated by panels of typical curve shapes for non-gated and gated transporters to enable a first classification of mechanisms. We demonstrate that all system parameters can be determined fairly well by fitting the model to "experimental" data of known origin. Applicability of the model to channels, pumps and cotransporters is discussed.

Keywords Current–voltage–time relationships · Enzyme kinetics · Ion transport · Multi-parameter fit · Voltage gating

D. Gradmann (✉)
Abteilung Biophysik der Pflanze,
Universität Göttingen,
Untere Karspüle 2,
37073 Göttingen, Germany
E-mail: dgradma@gwdg.de
Tel.: +49-551-397838
Fax: +49-551-397838

C. M. Boyd
Department of Oceanography,
Dalhousie University,
Halifax, NS, B3H 4J1, Canada

Introduction

Ion transporting proteins can be considered as enzymes catalyzing translocation of ions through lipid membranes between the two bulk solutions, inside ($_i$) and outside ($_o$) of a cytoplasmic compartment. In a special biochemical sense, enzymes break and form covalent bonds. Although this function does not strictly apply in general for ion transporters, their substrates are, in fact, debound and bound from and to hydronic water in the two bulk solutions before and after the main translocation step(s).

Kinetic aspects of many ion transporters have been worked out from the electrophysiological point of view, focusing on conductances (e.g. Neher and Stevens 1977; Läuger 1980, 1995; Bernèche and Roux 2001; Morais-Cabral et al. 2001). In contrast, saturation currents at large voltage deviations from equilibrium, which correspond to saturation velocities in classical enzyme kinetics, have not been studied with comparable effort, mostly because such saturation phenomena are not observed routinely by electrophysiologists. Nevertheless, in a general sense, ion transporters are enzymes and enzyme kinetics can therefore be assumed to apply for their operation in general, even for ion channels (Eisenberg 1990), which are mistakenly viewed sometimes as purely electrical devices in contrast to the metabolic devices of familiar enzymes. The subsummation of ion transporters, in particular ion channels, as enzymes requires some adjustments of focus and terminology:

Whereas in traditional enzyme kinetics, substrate and product have different structures and names, they differ just by location in the case of ion transporters. For

instance, depending on the sign of the thermodynamic gradient, a given internal substance S_i, which can be processed by a certain transporter, will be substrate in case of efflux and product in the case of influx.

Furthermore, electrophysiologists have coined many expressions with equivalent meanings in traditional enzyme kinetics, e.g. channel (high-turnover uniporter), carrier (low-turnover transporter), open (active), closed (inactive), gating (activation/deactivation), current (velocity), conductance (activity), uniporter (ordinary enzyme), pump (metabolic cosubstrate), cotransport (cosubstrate is also translocated).

In addition, the standard experimental configurations for traditional enzyme kinetics consist of excess substrate concentration, c_S, compared to the concentration of the product,c_P ($c_S/c_P >> 1$; key word: Michaelis–Menten), whereas internal and externalc_S of ion transporters are usually kept in the same range to ensure osmotically and thermodynamically well-defined conditions (key word: Nernst). In a superficial sense, electrophysiologists tend to focus on thermodynamic aspects and biochemists on kinetic ones. For an exhaustive analysis, however, thermodynamic *and* kinetic features must be considered equally well.

An important matter is the driving force. This is the substrate concentration in traditional enzyme kinetics. However, for ion transporters it is the electrochemical activity, consisting of an electrical component and a concentration term. This circumstance provides the possibility to obtain more experimental information about the system by changing the two components of the driving force systematically. Simplified, changing a concentration resolves a binding step, changing the voltage resolves the charge translocation, and saturation is defined by intramolecular steps of the reaction cycle, which are not affected by the voltage nor by the substrate concentrations.

In previous reports (e.g. Gradmann et al. 1987, 1997), the algorithms have been presented for solving this inverse problem, i.e. to determine the parameters (here the rate constants) of the active system from $I(V)$ curves recorded at various configurations of substrate concentrations.

The physiological currents I are, however, not only determined by the currents I_a through the active transporter, but as well by the active portion p_a of the whole population – or in microscopic terms the probability of an individual transporter molecule to be active:

$$I = I_a p_a \tag{1}$$

The activity p_a may, in turn, depend on V as well. This can be expected in general for membrane-spanning enzymes, because any charged residue is likely to cause voltage-dependent conformational changes in time with more or less expressed effects on the activity.

These changes in $p_a(V,t)$ are usually obtained from current recordings upon rectangular voltage changes (step protocols). Relatively long times are required for $I(V,t)$ recordings with complete I relaxations after each V step. In order to minimize disturbances of $I(V,t)$ records due to fluctuations and/or drifts of the electrical membrane properties, one can use triangular V protocols which allow complete $I(V,t)$ recordings in a much shorter time (Gradmann and Boyd 1999, 2000; Boyd et al. 2003).

In many experiments the operation of a transporter is documented by changes of the electrical characteristics of the membrane upon changing the external concentration of a putative substrate (e.g. Fingerle and Gradmann 1982). The difference of the electrical characteristics of the membrane $-dI(V)$ steady-state and $dI(V,t)$ dynamic – between the two concentration conditions can be used to determine the electrical characteristics of the transporter itself. This has been demonstrated in individual cases for steady-state (Maathuis et al. 1997) and for dynamic (Boyd et al. 2003) conditions. Warning: (unidirectional) $dI(V,t)$ records obtained by adding substrate outside are not identical with (net) $I(V,t)$ records of the transport itself.

This study presents a systematic overview about the possibilities and limits to obtain the kinetic system parameters of ion transporters using $dI(V,t)$ records from V-clamp experiments with triangular voltage protocols.

In general, $I(V)$ relationships of ion transport are non-linear. In order to discuss these non-linearities, we recall the general $I(V)$ equation of steady-state ion transport through an enzyme with an internal and an external charged state (occupancies p_i and p_o, with $p_i + p_o = 1$), one reversible reaction step (k_{io} and k_{oi}) of charge translocation, and a pair of global rate constants (κ_{io} and κ_{oi}) which represent the V-independent parts of the reaction cycle (Hansen et al. 1981):

$$I_a(u) = ze\frac{k_{io}\kappa_{oi} - k_{oi}\kappa_{io}}{k_{io} + k_{oi} + \kappa_{io} + \kappa_{oi}} \tag{2}$$

with the normalized membrane voltage $u = VF/(RT)$, where F, R, and T have their usual thermodynamic meanings, the charge number z of the transported substrate, and the elementary charge e; the voltage sensitivity of I_a is given by the rate constants $k_{io} = k_{io}{}^0 e^{zu/2}$ and $k_{oi} = k_{oi}{}^0 e^{-zu/2}$, where the superscript ^{0} marks the value of the rate constants at zero voltage, and 1/2 in the exponents marks a symmetric Eyring barrier.

In order to simplify the discussion of curvature, we normalize Eq. (2) by setting $z = 1$, $e = 1$, express rate constants as well as currents in dimensionless units, and assume symmetry for the moment: $k_{io}{}^0 = k_{oi}{}^0 = k^0$, and $\kappa_{io} = \kappa_{oi} = \kappa = 1$. So Eq. (2) becomes:

$$I_a(u) = \frac{k^0 e^{u/2} - k^0 e^{-u/2}}{k^0 e^{u/2} + k^0 e^{-u/2} + 2} \tag{3}$$

If $k^0 >> 1$, Eq. (3) degenerates to $I(u) = \sinh(u/2)$, where the current reaches half saturation at $u_{1/2} = \ln(3)$, corresponding to $\ln(3)RT/F \approx 27$ mV.

The other extreme, $k^0 << 1$ marks the behavior of a symmetric Eyring barrier where the current rises

exponentially with moderate voltages, and half saturation as well as maximum slope are reached at $u_{1/2} = 2\ln(2/k^0)$, from where on the current approaches saturation.

In comparison, the $I(V)$ relationship for $k^0 >> 1$ has just one inclination point in the origin, whereas for $k^0 << 1$ there are three: one in the origin and two at $+u_{1/2}$ and $-u_{1/2}$. In many experimental records, $u_{1/2}$ cannot be identified within the investigated voltage range. However, saturation is indicated in several experiments.

In principle, several mechanisms may limit the exponential increase. The simplest one, diffusion limitation, had earlier been excluded (Hille 1995), but has gained acceptance again in case of highly conductive K^+ channels (Bernèche and Roux, 2001; Morais-Cabral et al. 2001). In the case of diffusion limitation, saturation currents at $V << 0$ and $V >> 0$ are proportional to the substrate concentration in the source compartment. Another mechanism, known as "fast block", becomes effective when at increasing voltages non-transported ions with higher charge than the transported one (e.g. Ca^{2+} or Cs^+ compared to K^+; Klieber and Gradmann 1993) compete for the binding site more and more. This mechanism can be identified by its dependence on the concentration of the competing ions and by the fact that it does not come to rest at saturation currents but proceeds to complete suppression of the currents at large voltages. In enzymatic terms, this mechanism reflects competitive inhibition, where the electric component of the electrochemical activity of the non-transported competitor exceeds that of the transported substrate.

The third mechanism which counteracts exponential current increase with V is classical Michaelis–Menten saturation of enzymatic turnover by intrinsic properties of the enzyme itself. It corresponds to κ_{io} and κ_{oi} in Eq. (2) for given substrate concentrations inside (c_i) and outside (c_o). Calculations below will show the effect of c_i and c_o on the curvatures of the $I(V)$ curves according to Eq. (2). For the discussion of these curves the "relative steepness", $k_{io}k_{oi}/\kappa_{io}\kappa_{oi}$, has been introduced by Hansen et al. (1981). In terms of the simplified version of Eq. (3), there is a range of k^0 between $k^0 << 1$ and $k^0 >> 1$ where the shape of the $I(V)$ curves undergoes a transition between showing one and three inclination points. In this range of k^0 in Eq. (3) or $k_{io}{}^0k_{oi}{}^0/\kappa_{io}\kappa_{oi}$ in the general version of Eq. (2), the shape of the $I(V)$ curves can have a quasi-linear appearance over a relatively wide V range, which may account for experimental $I(V)$ curves with apparently little curvature.

The more familiar way, however, to account for weak curvatures in experimental $I(V)$ curves is dividing the single charge-translocating reaction step, described by $k_{io} = k_{io}{}^0e^{zu/2}$ and $k_{oi} = k_{oi}{}^0e^{-zu/2}$ in Eq. (2), into a series of $i = 1 \ldots n$ steps which are affected by correspondingly smaller fractions $\delta_j (0 < \delta_j < 1, \Sigma\delta_j = 1)$ of the entire voltage u. Let us assume the charge translocation from i to o in Eq. (2) is divided by an intermediate state M at the electrical distance $\delta = 0.5$ of the membrane. So the global rate constants $k_{io}' = k_{iM}k_{Mo}/(k_{Mi} + k_{Mo})$ and $k_{oi}' = k_{oM}k_{Mi}/(k_{Mi} + k_{Mo})$, as functions of the individual rate constants $k_{iM} = k_{iM}{}^0e^{zu/4}$, $k_{Mi} = k_{Mi}{}^0e^{-zu/4}$, $k_{Mo} = k_{Mo}{}^0e^{zu/4}$, and $k_{oM} = k_{oM}{}^0e^{-zu/4}$, will assume values of $k_{io}' = k_{iM}{}^0e^{zu/4}$ and $k_{oi}' = k_{Mo}{}^0e^{-zu/4}$ at large positive and negative voltages, respectively. We note smaller voltage sensitivity coefficients $d_{io}' = z/4$ and $d_{oi}' = -z/4$ in $k_{io}' = k_{io}{}^{0\prime}\exp(d_{io}'u)$ and $k_{oi}' = -k_{oi}{}^{0\prime}\exp(d_{oi}'u)$ compared with $d_{io} = z/2$ and $d_{oi} = -z/2$ of the one-step rate constants $k_{io} = k_{io}{}^0\exp(d_{io}u)$ and $k_{oi} = k_{oi}{}^0\exp(d_ou)$. In conclusion, dividing the charge translocation step in substeps will result in smaller amounts of the voltage sensitivity coefficients d, which means more linear $I(V)$ curves. Correspondingly, weak curvatures in $I(V)$ records indicate several serial steps for charge translocation.

However, the algebraically convenient assumption of *equal* steps is not justified without good reasons. In contrast, biological ion transporters are usually divided into pore-like sections (e.g. "mouths" in channels and F_0 particles in ATPases) with large k^0 values, and rate limiting catalytic sections with small k^0 values, such as a selectivity filter of low conductance channels and F_1 particles in ATPases (Junge et al. 1997). Of course, the pores are not homogeneous and the charge translocating step of the catalytic cycle may comprise a series of individual substeps again (Bernèche and Roux 2001; Morais-Cabral et al. 2001). However such details will hardly show up in the electrophysiological behavior of the total system.

With these considerations, we have developed a general model (Fig. 1) for gated ion transporters with a limited number (12) of independent system parameters (equilibrium constants, rate constants and their voltage sensitivity coefficients) which can be determined by fitting the model to experimental $I(V,t)$ relationships.

Materials and methods

Theory

Figure 1A shows an ordinary cyclic four-state reaction scheme for a transporter. Uneven state numbers denote states, which are oriented to the internal, cytoplasmic compartment and even numbers correspondingly denote orientation to the periplasmic space outside. Apparent rate constants for binding reactions are $k_{31} = k_{31}{}^0c'_i$ and $k_{42} = k_{42}{}^0c'_o$, where the superscript ^{0} marks the rate constants at reference conditions when all substrate concentrations are 1 mM, and c' is the concentrations (in mM) at the binding site of the enzyme. The binding reactions (k_{31}, k_{42}) and debinding reactions (k_{13}, k_{24}) are not marked explicitly because they are assumed to be much faster than the translocation reactions, k_{12},k_{21},k_{34} and k_{43}. They are represented, therefore, by equilibrium constants $K_1 = k_{31}/k_{13} = K_1{}^0c'_i$ and $K_2 = k_{42}/k_{24} = K_2{}^0c'_o$ for state 1 and state 2, respectively, where the superscript ^{0} denotes reference conditions ($c' = 1$ mM) again.

In thermodynamic equilibrium under reference conditions ($V = 0, c = c' = 1$ mM, denoted by ^{0}), microscopic reversibility dictates: $k_{12}{}^0k_{43}{}^0K_1{}^0 = k_{21}{}^0k_{34}{}^0K_2{}^0$. Thus only five of the six parameters $k_{12}{}^0$, $k_{21}{}^0$, $k_{34}{}^0$, $k_{43}{}^0$, $K_1{}^0$ and $K_2{}^0$ are independent. We have arbitrarily chosen the first five of this series to be independent and $K_2{}^0 = K_1{}^0k_{12}{}^0k_{43}{}^0/(k_{21}{}^0k_{34}{}^0)$.

Figure 1B illustrates the assumption that the entire transmembrane voltage, V, as measured between the two bulk phases, affects the transport cycle only by a portion $\delta_{tr} (0 < \delta_{tr} < 1)$, whereas δ_o and $\delta_i (\delta_{tr} + \delta_o + \delta_i = 1)$ mark an external and an internal V portion,

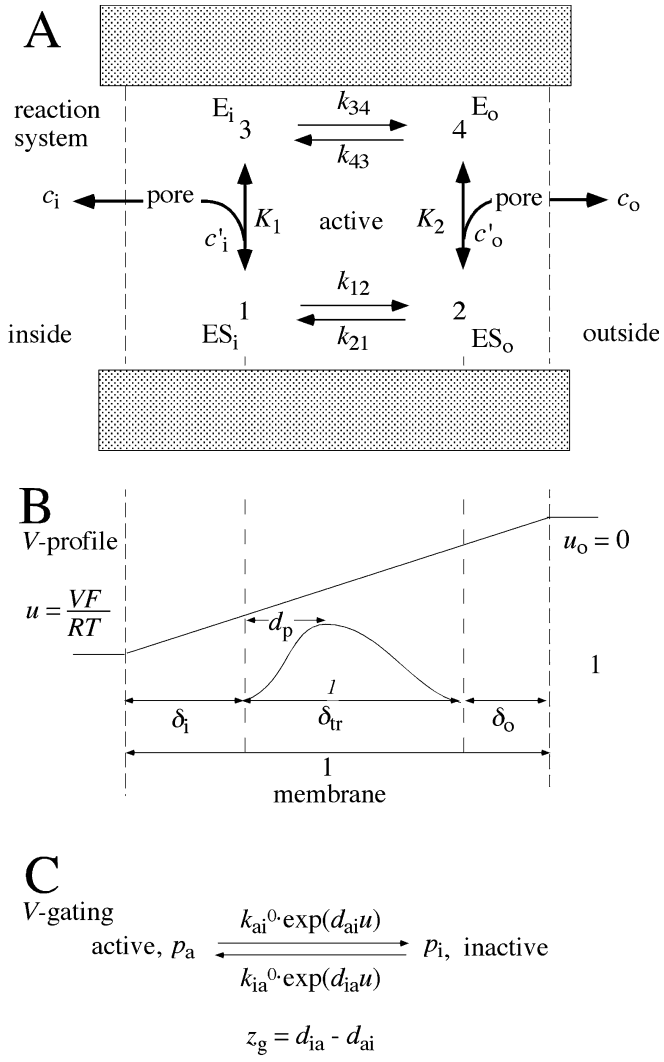

Fig. 1A–C Definition of model parameters used. **A** Enzymatic reaction cycle for an ion transporter, where the concentrationsc' at the binding sites may differ from the concentrations c in the bulk solutions; binding and debinding reactions are assumed to be fast compared to translocation steps. **B** Hypothetical voltage profile through the membrane, where the transporter experiences only a fraction $\delta_{tr} < 1$ of the entire voltage, V, and the remaining portion $(1-\delta_{tr})$ is ascribed to an inner and an outer portion, δ_i and δ_o, respectively. **C** Definitions for formal treatment of a simple mechanism for voltage-dependent changes of the activity of an enzyme (V gating)

respectively, which determines the difference between the concentrations c of an ion with the charge z in the bulk and c' immediately at the binding site of the translocating reaction cycle:

$$c'_o = c_o \exp(-z\delta_o u); \quad c'_i = c_i \exp(z\delta_i u) \tag{4}$$

The electrical distances δ_o and δ_i may reflect spatial differences through a conducting pore between the membrane surface and the enzymatic binding sites (Gradmann et al. 1997) and/or the effect of surface charges (Kinraide 2001). This formalism corresponds to the assumptions that charge translocation occurs by three major voltage-dependent steps in series, where the first and the last reflect fast equilibrations by electrodiffusion, and the central enzymatic cycle is rate limiting.

As for the V dependence of the enzymatic cycle, two theoretical model versions can be discriminated. For the corresponding considerations we assume a substrate with the charge number $z = +1$. In model version 1 (MV1), the empty enzyme (states 3 and 4) is electroneutral and the charge number $z = +1$ is assigned to the loaded enzyme (states 1 and 2). In model version 2 (MV2), the empty states 3 and 4 are assumed to be charged with $z = -1$, and the loaded states, 1 and 2, to be neutral. In MV1, V dependence is introduced by:

$$k_{12} = k_{12}^0 \exp(zd_p u); \quad k_{21} = k_{21}^0 \exp(z(d_p - 1)u) \tag{5}$$

where $z = 1$ is the charge number of the translocated species and d_p $(0 < d_p < 1)$ is the distance of the peak of the Eyring barrier with respect to its width (inside 0, outside 1). In MV2, V dependence of the reaction cycle is given by:

$$k_{34} = k_{34}^0 \exp(zd_p u); \quad k_{43} = k_{43}^0 \exp(z(d_p - 1)u) \tag{6}$$

with $z = -1$, and V-independent k_{12} and k_{21}.

The four steady-state occupancies:

$$p_1 + p_2 + p_3 + p_4 = 1 \tag{7}$$

can be determined from the four differential equations:

$$dp_1/dt = -(k_{12} + k_{13})p_1 + k_{21}p_2 + k_{31}p_3 \tag{8}$$

$$dp_2/dt = -(k_{21} + k_{24})p_2 + k_{12}p_1 + k_{42}p_4 \tag{9}$$

$$dp_3/dt = -(k_{31} + k_{34})p_3 + k_{13}p_1 + k_{43}p_4 \tag{10}$$

$$dp_4/dt = -(k_{42} + k_{43})p_4 + k_{24}p_2 + k_{34}p_3 \tag{11}$$

With the above assumption ($k_{12},k_{21},k_{34},k_{43} << k_{14},k_{41},k_{23},k_{32}$) and the stability constants, $K_1 = k_{31}/k_{13}$ and $K_2 = k_{42}/k_{24}$ (use of stability constants $1/K_D$ is sometimes more comfortable than dissociation constants K_D), these equations yield:

$$p_1 = F_1/den; \quad p_2 = F_2/den; \quad p_3 = F_3/den; \quad p_4 = F_4/den \tag{12}$$

with:

$$F_1 = K_1(k_{21}K_2 + k_{34}), \quad F_2 = K_2(k_{12}K_1 + k_{43}), \quad F_3 = k_{12}K_1 + k_{43}, \quad F_4 = k_{21}K_2 + k_{34} \tag{13}$$

and:

$$den = F_1 + F_2 + F_3 + F_4 \tag{14}$$

The current through the active reaction cycle corresponds to the net translocation rate in counterclockwise direction:

$$I_a = p_1k_{12} - p_2k_{21} = p_4k_{43} - p_3k_{34} \tag{15}$$

for both MV1 and MV2. The equality of Eq. (15) is a consequence of mass conservation (Eq. 7) in the steady state: in the closed reaction cycle, the net circulation must be the same everywhere.

In principle, when the rate constants k have their usual dimension of s^{-1}, the right-hand side of Eq. (15) has to be multiplied with the elementary charge, 1.6×10^{19} A s, a charge number and a stoichiometric coefficient to yield the current through an individual, active transporter molecule (compare Eq. 2). Since we do not know whether the recorded steady-state currents are due to a few transporter molecules with large k values or many transporters with small turnover, we simply leave Eq. (15) in its simple form and understand that the k values and the currents are normalized parameters without dimension. For $V << 0$ and $V >> 0$, Eq. (15) degenerates to simple expressions for the positive and negative saturation currents:

$$I_{S+} = k_{43}/K_2 \text{ and } I_{S-} = k_{34}/K_1 \tag{16}$$

respectively. Equations (16) mean that I_{S+} is independent of c_i, and I_{S-} is independent of c_o.

For complete, dynamic current–voltage–time relationships, the steady-state currents I_a of the active transporter have to be multiplied by the actual activity p_a (Eq. 1). For the present purpose, a

gating scheme is used with an active state (a) and an inactive one (i). The V-sensitive transition probabilities for the transitions from the inactive state to the active one and back are:

$$k_{ia} = k_{ia}^0 \exp(d_{ia}u); \quad k_{ai} = k_{ai}^0 \exp(d_{ai}u) \tag{17}$$

respectively, where the superscript ^{0} marks the value of k at zero voltage again, and d_{ia} and d_{ai} are voltage sensitivity coefficients for k_{ia} and k_{ai}, respectively. These voltage sensitivity coefficients for gating have opposite sign and add up to the apparent gating charge, $z_g = d_{ia} - d_{ai} = \delta_g z_{gp}$, i.e. activation/inactivation by displacement of a mobile gating domain with the true charge z_{gp} along the distance δ_g ($0 < \delta_g < 1$) through the entire electrical field ($= 1$) of the membrane.

The steady-state activity of the transporter is:

$$p_a = 1/(1 + k_{ai}/k_{ia}) \tag{18}$$

and upon a change in voltage from V_0 to V_1, p_a relaxes with the gating time constant:

$$\tau_g = 1/(k_{ia} + k_{ai}) \tag{19}$$

with k_{ia} and k_{ai} at V_1. In the present study, τ_g is not used explicitly. Here, the temporal changes in p_a have been calculated iteratively for small time increments dt using the differential equation:

$$dp_a/dt = -k_{ai}p_a + k_{ia}(1 - p_a) \tag{20}$$

Explicitly, p_a was calculated first by Eq. (18) for steady-state conditions at a start voltage (e.g. 0 mV); for changing voltages, 2 mV steps per time intervals $dt = 10$ ms were used to calculate the actual activity, $p_{a,act} = p_{a,prev} + dp_a$, iteratively with the previous activity $p_{a,prev}$ and the changes $dp_a = (-k_{ai}p_a + k_{ia}(1-p_a))dt$, using rearranged Eq. (20) with the k values at the actual voltage.

All calculations have been carried out with a PC using custom-tailored programs written in Turbo Pascal. The software is available on request.

Results

The model calculations presented here are designed to correspond to the experiments when a transporter of interest is identified and characterized by recordings of the electrical properties of the membrane in the absence and presence of the putative substrate with an assumed $z = 1$ in the experimental bath medium: first, I_o at $c_{o0} = 0$, and second, I_1 at $c_{o1} > 0$. The two records are assumed to take place within such a short time that the internal substrate concentration c_i does not change significantly. We also assume that the investigated membrane has some background electrical properties which do not change between the first and the second experiment. So in the first experiment, the contribution of the currents through the transporter of interest is not known; and the experimental information about the transporter has to be taken from the current differences, $dI = I_1 - I_0$, between the two experiments. In the presented examples these difference records are shown as bold curves, and the two parent records, from $c_{o0} = 0$ and $c_{o1} > 0$, as curves with fine and normal thicknesses, respectively. For steady-state conditions, the three corresponding $I(V)$ curves do not intersect with each other, because an increase of c_o will cause an increased influx at all voltages. Before considering gating, we focus first on steady-state conditions of the transport cycle.

Steady-state conditions of the transport cycle

For reference purposes (Fig. 2C), numerically very simple configurations have been chosen (symbols as marked in Fig. 1A, B; numerical values listed in Table 1, line 1):

1. δ_o, $\delta_i = 0$. This means $\delta_{tr} = 1$ and effect of the full transmembrane voltage on the catalytic reaction cycle.
2. All rate constants $= 1$ at $V = 0$.
3. Both apparent stability constants, K_1, $K_2 = 1$ at c_i, $c_o = 1$; K_1 independent, K_2 determined.
4. $dz = 0.5$, i.e. symmetric Eyring barrier for the charge translocating reaction step.
5. $c_i = 1$, $c_{o0} = 0$, before $c_{o1} = 1$.

From the reference records in Fig. 2C, some obvious relationships can readily be explained by Eqs. (13) to (15).

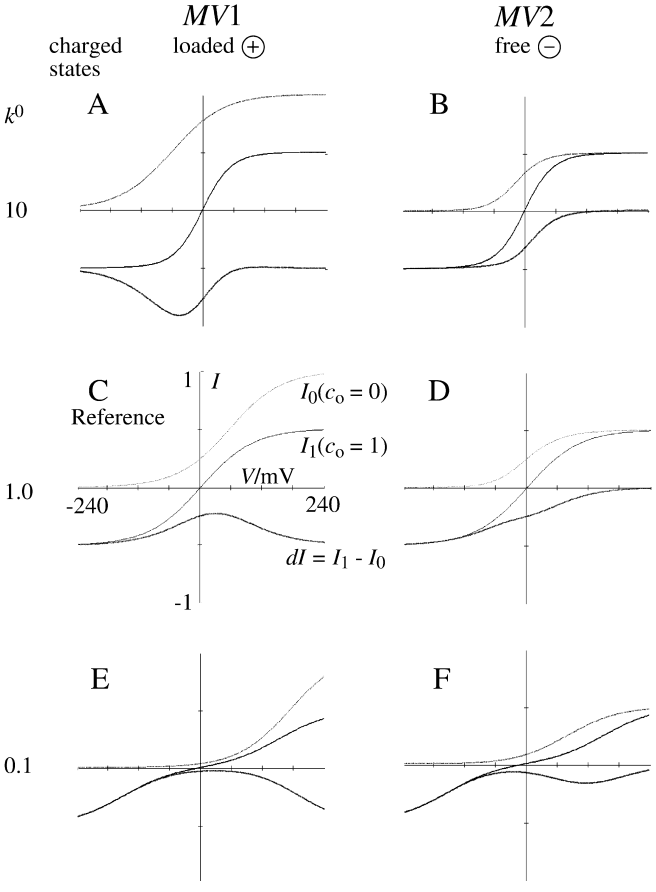

Fig. 2A–F Impact of velocity (descending order) of charge translocating reactions k^0 at $V = 0$, $k_{12}{}^0$, $k_{21}{}^0$ in MV1 (*left column*, electroneutral binding site and charged ($z = 1$) enzyme–substrate complex), and $k_{34}{}^0$, $k_{43}{}^0$ in MV2 (*right column*, charged ($z = -1$) binding site and electroneutral enzyme–substrate complex), compared to velocity of limiting, electroneutral reaction steps: k_{34}, k_{43} (MV1), and k_{12}, k_{21} (MV2), on the shape of steady-state $I(V)$ curves at $c_i = 1$ and $c_o = 0$ (I_0) or $c_o = 1$ (I_1), respectively, and on difference currents $dI = I_1 - I_0$. Explicit labelling of tracings and coordinates in reference panel **C**; analogous relationships in unlabeled panels. System parameters listed in Table 1

Table 1 Parameter configurations of model in Fig. 1 used for analysis of steady-state currents $I_a(V)$ of active transporter; definitions in Fig. 1; $c_{o1} > 0$ after $c_{o0} = 0$

No.	K_1^0	δ_{ir}	δ_o	d_p	k_{12}^0	k_{21}^0	k_{34}^0	k_{43}^0	c_i	c_{o1}	Figure	
											MV1	MV2
1	**1**	**0**	**0**	**0.5**	**1**	**1**	**1**	**1**	**1**	**1**	2C, 3A	2D, 4A
2	1	0	0	0.5	**10**	**10**	1	1	1	1	2A	
3	1	0	0	0.5	**0.1**	**0.1**	1	1	1	1	2E	
4	1	0	0	0.5	1	1	**10**	**10**	1	1	2B	
5	1	0	0	0.5	1	1	**0.1**	**0.1**	1	1	2F	
6	**10**	0	0	0.5	1	1	1	1	1	1	3B	4B
7	**0.1**	0	0	0.5	1	1	1	1	1	1	3C	4C
8	1	**0.5**	0	0.5	1	1	1	1	1	1	3D	4D
9	1	0	**0.5**	0.5	1	1	1	1	1	1	3E	4E
10	1	0	0	**0.9**	1	1	1	1	1	1	3F	4F
11	1	0	0	**0.1**	1	1	1	1	1	1	3G	4G
12	1	0	0	0.5	**10**	1	1	1	1	1	3H	4H
13	1	0	0	0.5	**0.1**	1	1	1	1	1	3I	4I
14	1	0	0	0.5	1	**10**	1	1	1	1	3J	4J
15	1	0	0	0.5	1	**0.1**	1	1	1	1	3K	4K
16	1	0	0	0.5	1	1	**10**	1	1	1	3L	4L
17	1	0	0	0.5	1	1	**0.1**	1	1	1	3M	4M
18	1	0	0	0.5	1	1	1	**10**	1	1	3N	4N
19	1	0	0	0.5	1	1	1	**0.1**	1	1	3O	4O
20	1	0	0	0.5	1	1	1	1	**10**	1	3P	4P
21	1	0	0	0.5	1	1	1	1	**0.1**	1	3Q	4Q
22	1	0	0	0.5	1	1	1	1	1	**10**	3R	4R
23	1	0	0	0.5	1	1	1	1	1	**0.1**	3S	4S

The fine I_o curve ($c_o = 0$) shows no inward currents, of course. Its $I_{S+} = 1$ reflects Eq. (15) with $p_3 = 0$ in the case of $c_o = 0$. The short-circuit current of 0.25 by Eq. (15) becomes evident when we recognize the occupancies $p_1 = 1/4$, $p_2 = 0/4$, $p_3 = 2/4$, and $p_4 = 1/4$ in Eq. (13) for $K_2 = 0$, and $k_{12}, k_{21}, k_{34}, k_{43}, K_1 = 1$.

The symmetrical I_1 curve ($c_o = 1$) of normal thickness has to pass the origin for thermodynamic reasons (no current in the absence of driving forces) and shows saturation currents of ± 0.5, reflecting the 50 : 50 equilibrium between the occupied and empty states of the binding site. With a little bit of algebra it can be derived from Eqs. (13) – (15) that the shapes of the I_0 and I_1 curves are identical. The two curves are only displaced from each other by 0.25 in the vertical direction, and in the horizontal direction by $u = 2\ln(3)$, corresponding to about +55 mV. So the maximum slope of the I_1 curve is in the origin and that of the I_0 curve at about 55 mV. This means that the difference curve rises at 0, falls at +55 mV, and has its maximum in between.

These relationships hold for that model version where the free binding site has the charge number $z = 0$ and the loaded one $z = +1$, which has arbitrarily been chosen as MV1, in contrast to MV2 where the charge of the free binding site is $z = -1$, and that of the loaded one $z = 0$.

The behavior of MV2 with corresponding reference parameter values (Fig. 2D) differs from that of MV1 fundamentally, in so far as I_{S+} of MV2 does not change with c_o. As a consequence, the c_o-induced, steady-state $dI(V)$ curves of MV2 will approach zero current for positive V. However, this approach is not necessarily monotonic (Fig. 2F).

Figure 2 demonstrates the steepness effect of the relative magnitude of the rate constants of the V-sensitive reaction steps (k_{12}, k_{21} in left column with MV1, and k_{34}, k_{43} in right column with MV2) as compared with the V-insensitive reaction steps, which are normalized to unity (k_{34}, k_{43} in MV1, and k_{12}, k_{21} in MV2). The reference configurations with V-dependent k values = 1 at $V = 0$ (k^0) are shown in the middle pair of plots (C and D), whereas the upper and lower pairs show the impact of the k^0 values, which are an order of magnitude larger (A and B) and smaller (E and F), respectively.

The examples in Fig. 2 illustrate the effects of catalysis (lowering an energy barrier, corresponding to an increase of the forward and backward reaction by a common factor) and allosteric inhibition (elevating an energy barrier, corresponding to a decrease of the forward and backward reaction by a common factor) within the charge translocating and electroneutral parts of the reaction cycle. For example, the change of shape of the dI curve from Fig. 2C to Fig. 2A may reflect catalysis of the charge translocating step (common increase of k_{12} and k_{21} by a factor of 10) or allosteric inhibition within the electroneutral part (e.g. common decrease of k_{34} and k_{43} by a factor of 10); the change of the absolute currents (increase or decrease) will tell, of course, which of the two possibilities is true.

We note that the I_1 curves (middle traces of normal thickness in each plot) are identical in both model versions for the symmetric configuration of rate constants and concentrations, and that they approach saturation faster with increasing k^0 values. By the same token, the smaller the k^0 values, the wider the V range in which the V-dependent reaction steps are rate limiting and shape forming for the $I(V)$ curve with their exponential V dependence (Eqs. 5, 6).

For a qualitative interpretation of experimental $dI(V)$ records it is interesting to note that each $dI(V)$ curve in Fig. 2 (lower, and bold curves) has its special shape. As for MV1, dI_{S+} and dI_{S-} approach finite, negative values. In the intermediate V range, dI passes a minimum, for large k^0 values (Fig. 2A), and a maximum for small k^0 values (Fig. 2C, E), which broadens with decreasing k^0values.

It has already pointed out that I_{S+} approaches zero in MV2. Here, large k^0 values cause a sigmoid $dI(V)$ curve (Fig. 2B). Moderate k^0 values (Fig. 2D) result in a monotonic $dI(V)$ curve with three inclination points; small k^0 values cause an N-shaped (non-monotonic) $dI(V)$ curve (Fig. 2F). If under experimental conditions the accessible V range is not as wide as in Fig. 2, the $dI(V)$ curve of the type in Fig. 2F may show only a maximum and could be misinterpreted, therefore, to be of the type in Fig. 2C or Fig. 2E. However additional tests (see below) allow an unequivocal assignment to MV1 or MV2 also in such cases.

Figs. 3 and 4 show the effects of individual model parameters on the shape of the steady-state $I(V)$ curves

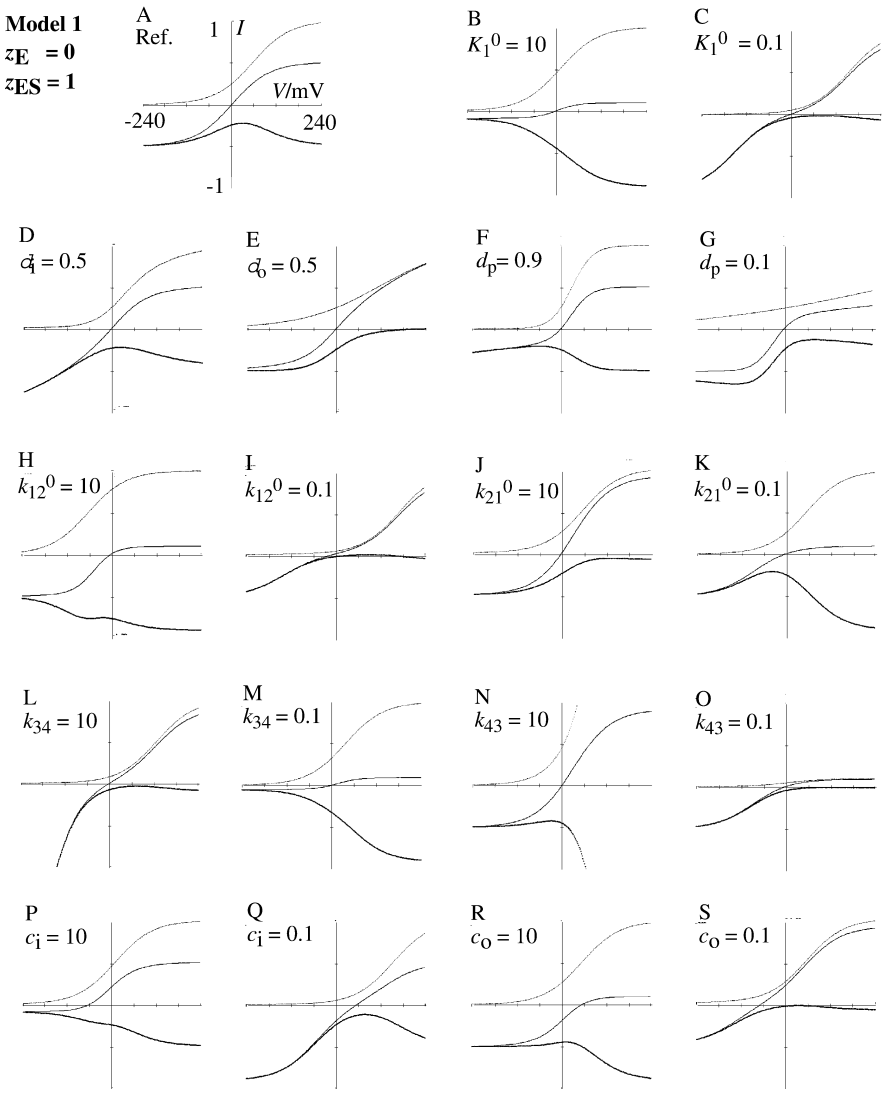

Fig. 3A–S Impact of individual system parameters in MV1 on shape of steady-state $I(V)$ curve; standard (if not labeled otherwise):$c_i = 1$ and$c_o = 0$ (I_0) or $c_o = 1$ (I_1), respectively, and on difference currents $dI = I_1 - I_0$. Explicit labelling of tracings and coordinates in reference panel **A**; analogous relationships in unlabeled panels. Parameters listed in Table 1

of I_0, I_1 and dI in MV1 and MV2, respectively. For reference purposes, the panels A in Figs. 3 and 4 correspond to the reference plots in Fig. 2C and Fig. 2D, with the default parameter configuration in Table 1, line 1. It would be long-winded to discuss each of the 36 plots explicitly. Only some qualitative features can be pointed out.

Model version 1

Let us focus on MV1 (Fig. 3) first, and note some observations.

1. None of the examples of this model version shows an N-shaped $dI(V)$ curve.
2. The dI currents in the far negative V range reflect inward currents, whereas in the far positive V range, the dI currents reflect suppression of outward currents.
3. Each example shows a characteristic $dI(V)$ curve, except Fig. 3B and Fig. 3M which are similar, although not identical.
4. Figure 3B and Fig. 3C show the effect of the equilibrium constant for binding under reference conditions ($V = 0$, and 1 mM substrate concentrations). An increase (Fig. 3B) reduces the availability of empty binding sites (inhibition of outward current upon addition of external substrate), and a decrease (Fig. 3C) stimulates it correspondingly. The shapes of the I_1 curves correspond to a large (Fig. 3B) and a small (Fig. 3C) k^0 in Eq. (3). In other words, large stability constants for the charged states exert more weight on the voltage-dependent part of the reaction cycle, so it will be less rate limiting.
5. Figures 3D and Fig. 3E demonstrate (i) that the curvatures of the $I(V)$ curves become less pronounced, of course, when the reaction cycle is exposed to only a fraction (here 50%) of the total V, and (ii) that the position of the active site (reaction cycle) of the enzyme within the electric field of the membrane causes an asymmetric flattening of the parent $I(V)$ curves. For instance, the I_1 curve of Fig. 3D shows less curvature at negative than at

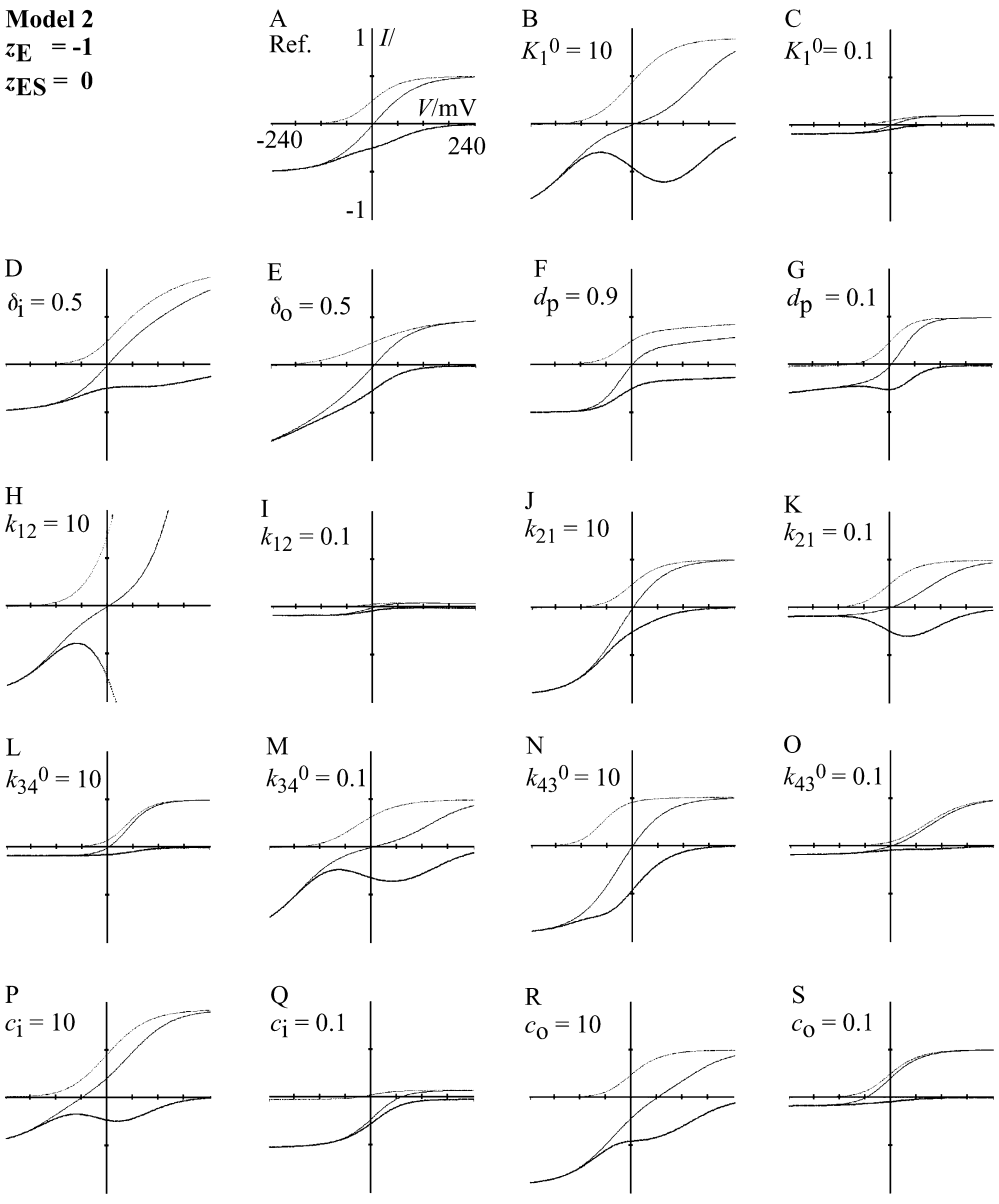

Fig. 4A–S Impact of individual system parameters in MV2 on shape of steady-state $I(V)$ curve; standard (if not labelled otherwise): $c_i = 1$ and $c_o = 0$ (I_0) or $c_o = 1$ (I_1), respectively, and on difference currents $dI = I_1 - I_0$. Explicit labelling of tracings and coordinates in reference panel **A**; analogous relationships in unlabeled panels. Parameters listed in Table 1. Note: in this model version, $I_0(V)$ and $I_1(V)$, approach the same saturation, I_{S+}, at $V>>0$

positive V, when the transporter is located in the external half of the electric field. Interestingly, the dI curve in Fig. 3E approaches zero, just as in MV2 (Fig. 4). The reason for this atypical behavior of dI in Fig. 3E is vanishing of c'_o (Eq. 4) at large positive voltages.

6. Similarly, the asymmetry of the Eyring barrier (Eq. 5) affects the curvatures of the $I(V)$ curves differently in the positive and in the negative branches. For example, a peak distance d_p of 0.9 in Fig. 3F means that k_{12}, which is proportional to the unidirectional outward current, is more affected than k_{21} for the inward current. Correspondingly, the I_1 curve shows a strong curvature for the outward current (positive) and a weak curvature for inward currents. Alternatively, the small slope of the I_0 curve in Fig. 3G reflects the small voltage-sensitivity coefficient $d_p = 0.1$ for the outward current. With respect to the reference dI curve with a symmetrical Eyring barrier ($d_p = 0.5$) in Fig. 3A, the asymmetry of the Eyring barrier in Fig. 3F and Fig. 3G is reflected in the experimental dI curves by the asymmetric shapes by which the current changes from its peak (minimum inward current) to its final level, −0.5 at $V<<0$ and $V>>0$.
7. The following discussion of the impact of the individual rate constants k_{12}, k_{21}, k_{34} and k_{43} on the shape of the $I(V)$ curves (Fig. 3H to Fig. 3O) cannot be carried out without corresponding changes of the dependent stability constant:

$$K_2^0 = K_1^0 k_{12}^0 k_{43} / \left(k_{21}^0 k_{34}\right) \tag{21}$$

Since under reference conditions, when all rate constants as well as K_1^0 are 1, the I_1 curves have to pass the origin for thermodynamic reasons, a tentative accel-

eration of the reaction cycle in counterclockwise direction, e.g. by k_{12}^0, has to be compensated by a corresponding increase of K_2^0 which points in the clockwise direction. So the indicated changes of individual rate constants in Fig. 3H to Fig. 3O are accompanied by corresponding changes of K_2^0, i.e. parallel in the case of k_{12}^0 and k_{43}, and antiparallel in the case of k_{21}^0 and k_{34}.

8. Correspondingly, acceleration (retardation) of the charge translocating step k_{12} in Fig. 3H (Fig. 3I) puts more (less) weight on the charged state 2, simultaneously by k_{12} and by K_2, which results in a very large (small) slope for I_0 and I_1. The characteristics of the bold dI curve in Fig. 3H for 10-fold k_{12} (and K_2), compared to the reference configuration in Fig. 3A, comprises large but not very V-sensitive currents that stretch from −0.5 for $V<<0$ to −0.9 for $V>>0$, and show three inflection points in between. The dI curve for small k_{12} (Fig. 3I) is similar to that of Fig. 3C but saturates only at −0.5 for $V<<0$.
9. The effects of changes in k_{21} are not equivalent, nor even symmetrical to the corresponding changes in k_{12} discussed in the previous paragraph, because changes in k_{21} go along with inverse changes in the stability constant K_2. Correspondingly, the increase of k_{21} (and simultaneous decrease of K_2) causes a sigmoid dI curve (Fig. 3J), which saturates much earlier and faster for $V<<0$ than the dI curve in Fig. 3I. Finally, a decreasedk_{21} (and simultaneously increased K_2) results in a similar, bell-shaped dI curve (Fig. 3K) as in the reference case (Fig. 3A), but asymmetric due to a saturation value of −0.9 at $V>>0$, compared with a symmetric one of −0.5 in Fig. 3A.
10. As for the V-insensitive reactions with k_{34} and k_{43}, the saturation currents I_{S-} and I_{S+} are determined by these rate constants together with the stability constants K_1 and K_2 (Eq. 16). Correspondingly, I_{S-} of I_1 in Fig. 3L and I_{S+} of I_0 in Fig. 3N curves as well as the (always negative) dI currents exceed the standard I coordinates of ± 1 of these plots of Fig. 3. We note that the dI curve for decreased k_{43} in Fig. 3O is very similar to the dI curve in Fig. 3I for decreased k_{12}. A major reason for this similarity is the common effect of a simultaneous decrease in K_2 in these two cases. A similar relationship can be identified if we compare Fig. 3K and Fig. 3M. The strongest similarity, however, exists between Fig. 3B and Fig. 3M. Closer inspection shows that this similarity is not an identity. Nevertheless, the small differences cannot be used to assign experimental data of this type to one of the two configurations.
11. Whereas the preceding cases refer to intrinsic features of the reaction cycle, the following effects of different c_i and c_o are under the control of the experimenter. There is a simple pattern in the changes of the dI curves upon rising or lowering c_i or c_o with respect to the reference situation (Fig. 3A): larger (smaller) c_i values cause dI to saturate at larger (smaller) amounts at $V<<0$, and vice versa, larger (smaller) c_o values cause dI to saturate at larger (smaller) amounts at $V>>0$ (Fig. 3P to Fig. 3S). In many cases, changes in c_i are of mere academic interest because they are difficult if not impossible to be performed in living cells. However, changes inc_o are usually well under the control of the experimenter.

Model version 2

Figure 4 shows the properties of this model version. It has already been pointed out that the common and characteristic feature is dI = 0 for $V>>0$. Also characteristic, but not throughout for MV2, is a V range where the d$I(V)$ curve has a negative slope between positive slopes, which causes an N-shape (panels B, G, H, K, M, and P in Fig. 4). One can discuss and understand the individual panels qualitatively again by the same rules that have been applied to MV1 (Fig. 3), especially by considering the distribution of impact between the$V$-sensitive part of the reaction cycle (here states 3 and 4) and the V-insensitive one (here states 1 and 2). Within the examples shown in Fig. 4, considerable similarities in the shapes of the dI curves can be seen in several panels such as A/O/R, B/M, C/I, D/R, and L/P/S.

Important for the experimenter is the behavior of dI upon changing concentrations c_o: in this MV2 the saturating amount of dI = 0 is independent of c_o, of course, but for $V<<0$ it rises and falls with increasing and decreasing c_o, respectively. In contrast, MV1 shows the opposite behavior of the saturating dI for large V displacements from 0 (Fig. 3R, S). Here, dI is independent of c_o at $V<<0$, but rises and falls in parallel with increasing and decreasing c_o at $V>>0$.

Summarizing the results from Fig. 3 and Fig. 4, we note that, in general, typical features of the reaction system are reflected by typical qualitative phenomena in the observable steady-state $I(V)$ curves. So it is not subtleties but remarkable differences already in the dI records by which intrinsic properties of the model can be identified. In principle, all details are implied in the above equations, but the collection of examples in the two figures (Fig. 3 and Fig. 4) may enable a first and quick assignment of experimental observations to basic properties of the system.

Dynamic gating

For dynamic conditions (definitions in Fig. 1C, same steady-state parameters as before) the additional reference parameters (Table 2, line 2) are: symmetric $k_{ai}^0 = k_{ia}^0 = 0.01\ s^{-1}$at $V = 0$, corresponding to relaxation times $\tau = 1/(k_{ai}+k_{ia})$, $\tau^0 = \tau_{max} = 50$ s at $V = 0$, which are larger than the time t_r (here, 4.8≈5 s)

for recording an $I(V,t)$ relationship. The V-sensitivity coefficients $d_{ai} = -d_{ia} = 0.5$ mean an apparent gating charge $z_g = d_{ia} - d_{ai} = -1$ and a symmetric Eyring barrier for V-gated inactivation.

The temporal and V-sensitive behavior of p_a in Eq. (1) is defined for the simple two-state (active and inactive) scheme in Fig. 1C by Eqs. (18)–(20). The behavior of p_a of a simple inward rectifier ($0 > z_g = d_{ia} - d_{ai} = -1$) during triangular V-clamp experiments is illustrated in Fig. 5. The five tracings A to E are calculated for a symmetric Eyring barrier (Eq. 17) with $d_{ai} = 0.5$, $d_{ia} = -0.5$, and $k^0 = k_{ai}{}^0 = k_{ia}{}^0$. The rate constants $k_{ai}{}^0 = k_{ia}{}^0 = k^0$ of 0.001–10 s^{-1}, as listed in Table 2, lines 1 to 5, correspond to relaxation time constants $\tau^0 = 1/(2k^0)$ at $V = 0$ of 500 to 0.05 s, respectively. In Fig. 5, these time constants are given as τ^0/t_r values with respect to our standard time $t_r \approx 5$ s of a recording cycle. The results for different k^0 at constant t_r equally reflect the effect of different recording speeds for a given k^0. The width between the upper and lower p_a values of a tracing in Fig. 5 marks the modulation depth ($1 - p_{a,lower}/p_{a,upper}$) at a given V.

For all tracings in Fig. 5 the maximum modulation depth is at $V = 0$, because the smaller one of the two temporal differences between the upper and lower values has a maximum there, under the actual conditions. As for the individual tracings with different τ^0/t_r, the modulation depth is a maximum function. At the reference voltage, $V = 0$, the modulation depth is only a few percent in tracing A with $\tau^0/t_r{}^0 = 100$, when the changes inp_a are too slow to follow the fast V protocol. Down to $\tau^0/t_r = 10$ (tracing Fig. 5B), the modulation depth rises roughly in proportion to falling τ^0/t_r, and shows a range of almost constant modulation depth of about 30% between −120 mV and +120 mV (except the discontinuity a $V = 0$ between the start and end of the record at $\tau^0/t_r = 1$ (Fig. 5C), the modulation depth has almost its theoretical maximum of 1.0. For even smaller τ^0/t_r (tracings D and E), the modulation depth decreases again due to contraction of the $p_a(V,t)$ tracings in the V direction. The absolute levels of p_a fall quickly from about 0.9 at −60 mV to about 0.1 at +60 mV in the nearly saturating case (Fig. 5E) with $\tau^0/t_r = 0.01$.

Table 2 Parameter configurations for analysis of V- and time-dependent activation/inactivation (V-gating) of transporters; definitions in Fig. 1C

No.	$k_{ai}{}^0(s^{-1})$	$k_{ia}{}^0(s^{-1})$	τ^0 (s)	d_{ai}	d_{ia}	Figure
1	**0.001**	**0.001**	500	+0.5	−0.5	5A
2	**0.01**	**0.01**	**50**	**+0.5**	−0.5	5B, 6A
3	**0.1**	**0.1**	5	+0.5	−0.5	5C
4	**1.0**	**1.0**	0.5	+0.5	−0.5	5D
5	**10**	**10**	0.05	+0.5	−0.5	5E
6	**0.05**	**0.05**	10	+0.5	−0.5	6B
7	**0.05**	0.01	17	+0.5	−0.5	6C
8	0.01	**0.05**	17	+0.5	−0.5	6D
9	0.01	0.01	50	**+0.4**	−0.6	6E
10	0.01	0.01	50	**+0.6**	−0.4	6G
11	0.01	0.01	50	−0.5	+0.5	6H

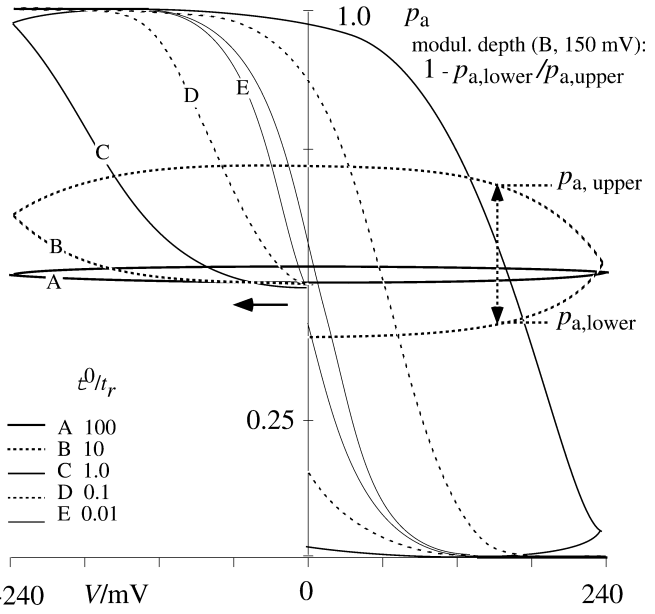

Fig. 5 Impact of recording time,t_r, of triangular$V$-clamp experiments, compared to magnitude of rate constants for V gating (expressed as relaxation time $\tau^0 = 1/(2k^0)$ at $V = 0$), on shape of V- and time-dependent activity $p_a(V,t)$ from triangular V-clamp experiments, plotted in $p_a(V)$ coordinates; here, the same values k^0 at $V = 0$ for k_{ia} (activation) and k_{ai} (inactivation); example configuration for inward rectifier with voltage-sensitivity coefficients $d_{ia} = -0.5$ and $d_{ai} = 0.5$, respectively, amounting to an apparent gating charge $z_g = d_{ia} - d_{ai}$ of −1

The combined V dependencies of the two non-linear expressions of I_a (Eq. 15, Figs. 2, 3, 4) and p_a (Eqs. 17, 18, 19, Fig. 5) have been calculated from the complete $I(V,t)$ relationships (Eq. 1, in Fig. 6); we use the reference steady-state model with the default parameters as in Fig. 2C = 3A for I_a in Eq. (1), and the $p_a(V,t)$ curve B with $\tau^0/t_r = 10$ in Fig. 5 for gating (Fig. 6A, Table 2, line 2).

The corresponding V protocols are indicated as an inset in the lower left quadrant of each panel of Fig. 6. In the upper left quadrants, the numerical configuration for the gating process are listed, and in the lower right quadrants are the time courses of p_a during the particular experiment. The temporal order of the results of the hypothetical V-clamp experiments is marked by arrows. The three records in each main panel of Fig. 6 comprise again a fine tracing I_o for $c_i = 1$ and $c_o = 0$, a normal one I_1 for $c_i = 1$ and $c_o = 1$, and a bold one for $dI = I_1 - I_0$.

For an interpretation of the plots in Fig. 6 we start with a comparison of I_0 with changing p_a in Fig. 6A, and I_0 with constant $p_a = 1$ in Fig. 3A. Under the given conditions ($k_{ia}{}^0 = k_{ai}{}^0$, $V_o = 0$), p_a equals $1/(1 + k_{ai}{}^0/k_{ia}{}^0) = 0.5$ at the beginning of the experiment; this means that I_o in Eq. (16) (Fig. 6A) starts with 0.5 of $I_a = 0.25$ in Fig. 3A, i.e. 0.125. Since with the given V protocol, Vmoves first to $V < 0$, p_a will rise from 0.5 towards 1 until V_1 is reached. During the following ascending branch of V from $V_1 < 0$ to $V_2 > 0$, p_a will first slow down its increase then keep a certain level for some

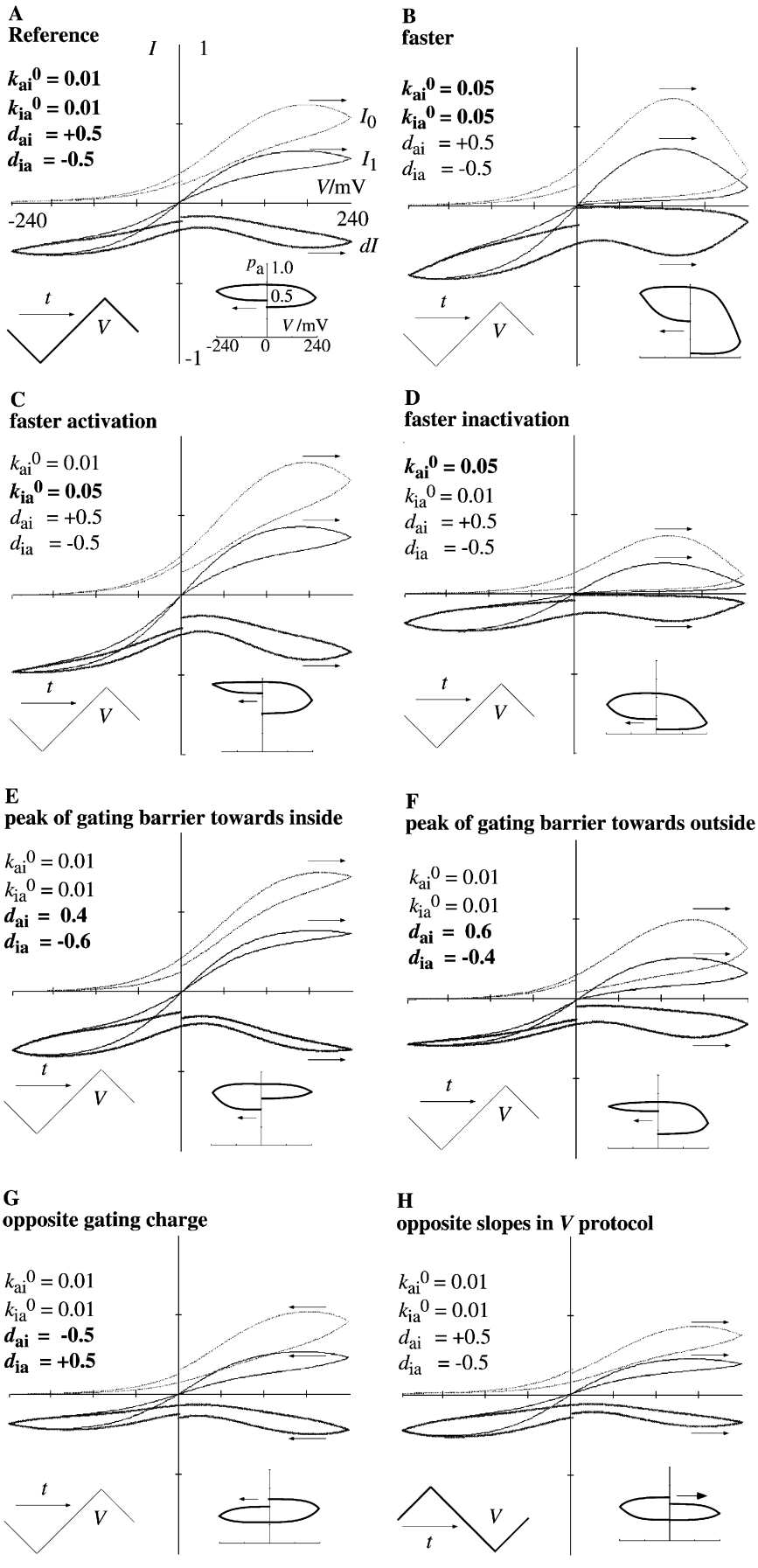

Fig. 6A–H Impact of gating parameters k_{ia}, k_{ai}, d_{ia}, d_{ai} and Vprotocol on $I(V,t)$ and $dI(V,t)$ from triangular V-clamp experiments with a V-gated transporter having a reference steady-state $I_a(V)$ of the fully active enzyme, as listed in Table 1, line 2; main panels comprise subpanels of a central $I(V,t)$, numerical configuration (*upper left*), schematic V protocol (*lower left*), and $p_a(V,t)$ plots (*lower right*). Explicit labelling of tracings and coordinates in reference panel **A**; analog relationships in unlabeled panels. Parameters listed in Table 1

time and decrease continuously from its maximum between 0.5 and 1.0 in the V range around $V = 0$. Upon the second sign change at $V_2 = +240$ mV, the decrease of p_a slows down and p_a reaches a minimum below 0.5, from where it rises towards the final $p_a = 0.5$ at $V = 0$ (not visible in the given presentation).

As for the I_1 tracing in Fig. 6A, the behavior of p_a is identical to that of I_0, but its I_a characteristics differ significantly from that of I_0 (Fig. 3A). We note that the loop of the I_o tracing at $V > 0$ is wider at than the loop of the I_1 tracing. This is not a gating effect but a simple scaling effect corresponding to the different I_{S+} values of the active transport cycle at $c_o = 0$ and $c_o = 1$ (see Fig. 2C = 3A). Nevertheless, these different widths determine the sign and amplitude of the width of the bold tracing $dI = I_1 - I_0$. We recall that $I(V,t)$ tracings of a V-gated transporter from triangular V-clamp experiments show an internal crossing at the reversal voltage of the transport process (Gradmann and Boyd 1999). In our case, this crossing takes place at $V = 0$ for I_1, and never for I_0.

It might appear puzzling that the dIcurves in Fig. 6 do not show internal crossing, although at least one of the parent $I(V,t)$ records (both would if c_o were not be totally absent but only reduced in the control experiment I_0) does intersect at the reversal voltage. This feature of dI explains the uniform negative sign of the dI_a (Fig. 3A) and the missing intersections in the $p_a(V,t)$ insets ($0 < p_a < 1$). The effects of the individual parameters of the gating scheme (Fig. 1 C) are illustrated by separate panels in Fig. 6, where panel A with its simple parameter configuration (Table 2, line 2) serves as a reference. Figure 6B with respect to Fig. 6A reflects the differences in recording/gating time, $\tau^0/t_r = 10$ and $\tau^0/t_r = 100$ in Fig. 5B and Fig. 5C. With increasing velocity of activation/inactivation, the loops become progressively wider for a given recording speed, i.e. the modulation depth reaches almost to 100% at some $V > 0$. Corresponding effects of even smaller and larger τ^0/t_r ratios can readily be derived from Fig. 3A and Fig. 5, and are not illustrated explicitly.

An increase of only k_{ia} (Fig. 6C), which would correspond to a decrease of the mean closed time in channel kinetics, causes an upscaling of the parent $I(V,t)$ curves I_0 and I_1 (mean activity increased) with an apparent increase of the modulation depth in the positive V range from about 25% (Fig. 5A, inset) to about 50% (Fig. 6C, inset), whereas in the negative V range the modulation depth decreases slightly from about 25% to about 20%. However, equivalent changes in modulation depth upon a sole increase of k_{ai} (Fig. 6D) cannot be confirmed. Here, the effect of increased k_{ai} corresponds to a downscaling of the $I(V,t)$ curves compared to Fig. 6B, which would correspond to a decreased mean lifetime of the active state.

The electrical distance of the barrier peak d_{ai} ($0 < d_{ai} < 1$) from the internal border of the gating barrier (width = 1) has a significant effect on the $I(V,t)$ records. Whereas the reference curve (Fig. 6A) with a symmetric barrier ($d_{ai} = 0.5$, $d_{ia} = -0.5$) shows about the same modulation depth of 25% in the positive and negative V ranges, a 10% shift of the barrier peak towards the inside ($d_{ai} = 0.4$, $d_{ia} = -0.6$, Fig. 6E) causes the modulation depth to increase significantly in the negative Vrange and to decrease in the positive Vrange correspondingly (see Fig. 6E, inset). A consequence of this asymmetry is that in this case the final current dI becomes more negative than dI in the beginning of the experiment (reason: corresponding behavior of I_0 because of $I_1 = 0$ at $V = 0$, at start and end).

The corresponding effects take place if the barrier beak is located 10% out of the middle towards the external side (Fig. 6F). Here the width of the loop (modulation depth of p_a in inset) is markedly increased in the positive V range and correspondingly decreased in the negative one.

This localization of the barrier peak by the asymmetry of the modulation depth at $V << 0$ and $V >> 0$, appears to be very convenient. It is pointed out, however, that the dI curves and the $p_a(V,t)$ insets of Fig. 6C and Fig. 6F are similar. So if the experimental data show a larger modulation depth in the positive V range compared to the negative one, additional criteria must be used to decide whether this effect is due to an increased k_{ia} (Fig. 6C) or due to a barrier peak in the external half of the electric field (Fig. 6F). In our case, the former shows more curvature in the positive loop.

The sign of the apparent gating charge ($z_g = d_{ia} - d_{ai} > 0$: outward rectification; $z_g = d_{ia} - d_{ai} < 0$: inward rectification) can be assessed quite easily by the behavior of the $I(V,t)$ curves in the vicinity of V_1 and/or V_2 when the slope dV/dt changes its sign. For instance, around the sign change at $V > 0$, the incident currents I_0 and I_1 of the inward rectifier under consideration will always exceed the reflected currents, and vice versa. Because of $I_0 > I_1$, the incident $dI = I_1 - I_0$ of the inward rectifier will be more negative than the reflected dI around the sign change at $V > 0$. Figure 6G shows the corresponding properties of an outward rectifier that differs from the reference model (Fig. 6A) only by the sign of the gating charge.

Finally, Fig. 6H illustrates that the order of the V protocol (starting with negative or positive dV/dt slope) has only a minor effect on the results. Actually, the small differences between Fig. 6A and Fig. 6H would vanish completely if not the first cycle of the triangular V protocol were considered but a following one.

Determination of system parameters

A good model should not only be able to describe experimental phenomena with a unique set of parameters. In several cases (Gradmann and Boyd 2000; Boyd et al. 2003) we obtained apparently suitable sets of parameters for some transporters by fitting the model to experimental data. Some reasons for the validity of the solutions have been provided. However, it has not been

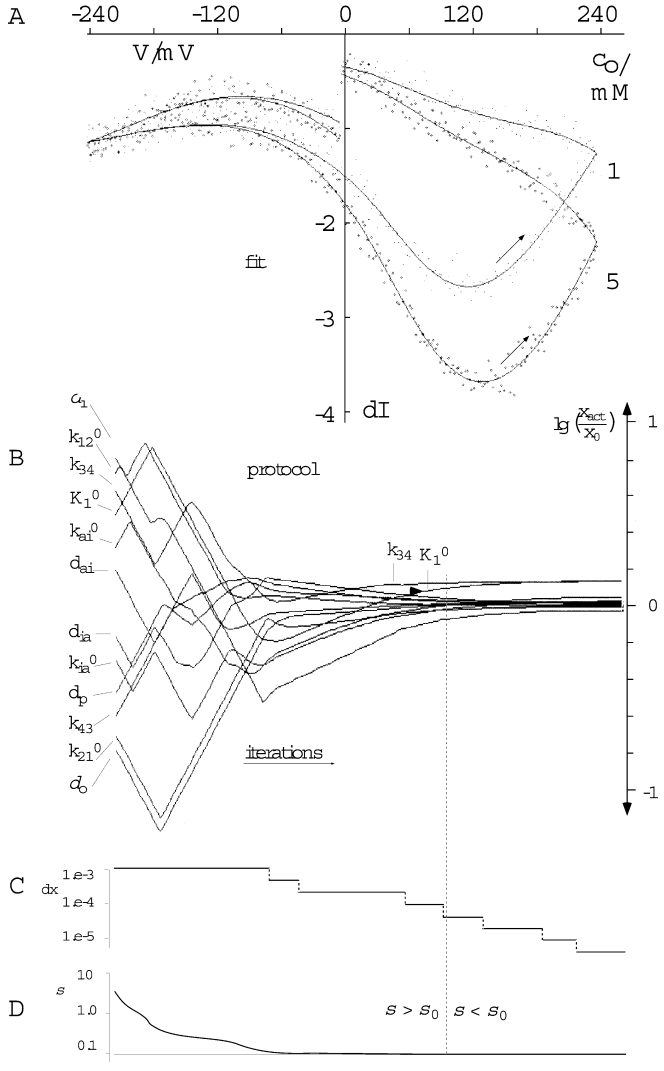

Fig. 7A–D Identification of model parameters by fit of model to hypothetical set of data. **A** Points: "true" data generated with model parameters x_0 as listed in Table 3 (columns a, b), and two different $c_o > 0$ ($c_o = 1$, small dI points; $c_o = 5$, large dI points); experimental: dV/dt slopes: ± 0.2 V s^{-1}; $V_0 = 0$ mV, $V_1 = -240$ mV, $V_2 = +240$ mV; superimposed gaussian noise: $\sigma_0 = 0.1$; 480 data points per sweep (whole cycle); curves: fitted records. **B** Fit protocol; temporal development of individual model parameters in the course of the fit; details of numeric configuration and algorithm in text; note: non-monotonic approximations. **C** Protocol of magnitude of fit increment dx common to the approximation of every parameter. **D** monotonic convergence of mean square error, σ, from initial 4.03 to $\sigma < \sigma_0$

demonstrated explicitly that the solutions are unique. Here, this problem is examined the following way. Hypothetical d$I(V,t)$ data (points in Fig. 7A) are generated by the model with an original, "true" set of parameters x_0 (Table 2C) and some superimposed gaussian noise σ_0. Then another set with different values x_1 has been chosen as start parameters for a least-squares fit routine with the goal to adjust the parameter set x iteratively to describe the "experimental" data well. Fits were only considered to be good if they converged to a final mean square deviation σ below the superimposed noise ($\sigma < \sigma_0$). In cases when x_1 differed too much from x_0 (e.g. by an order of magnitude and more), the fit routine converged to $\sigma > \sigma_0$ with an irrelevant set of parameters. The critical question about acceptable fits ($\sigma < \sigma_0$) was whether they converge towards the correct parameter setx_0. Alternatively, if the model has more independent system parameters than observable ones, the fits are expected to converge to ambiguous families of solutions where, for example, only some ratios between parameters are defined by the experimental data but the individual parameters may diverge. Acceptable fits with the presented model do not lead to such ambiguities but converge to a parameter set x which reflects the original set x_0 within the limits of the scatter. Figure 7B shows the history of such a fit with the 12 independent system parameters of the model.

Our experiences with various fit algorithms showed that fast algorithms with gradient-related fit increments (e.g. Marquardt–Levenberg, Simplex) do not yield as reliable results as the direct and slower algorithm of Hookes and Jeeves (1961), which runs repeatedly through all parameters with a fixed increment dx, and is reduced to 50% each time the fit does not improve anymore (Fig. 7C). The fit stops when dx becomes smaller than a given limit, e.g. 1×10^{-5} in the example of Fig. 7. Starting with too large dx causes the fits to converge towards unacceptability ($\sigma > \sigma_0$).

For the present example (Fig. 7), the system parameters x_0 (Table 3, column b) have been chosen arbitrarily (sort of reflecting the order of listing), but $\neq 1$ to keep the system non-degenerated by ambiguities. The choice of the start parameters for the fit (Table 3, column c) also followed an arbitrary pattern (similar distances in a logarithmic scale for convenient labelling in Fig. 7B).

Table 3 Protocol of fit in Fig. 7; column a: model parameters; column b (x_0): original values; column c (x_{start}/x_0): arbitrary factors of initial deviation from original ("true") parameters used to define start parameters for fit; column d (x_{fit}): fitted parameter values; column e (x_{fit}/x_0-1): deviations between fitted and "true" parameters, given in %. Gaussian noise of $\sigma_0 = 0.1$ was added to theoretical model currents; mean deviation σ between fitted data and noisy model data was 4.033 at the start and 0.099 at the end of the fit

a	b x_0	c x_{start}/x_0	d x_{fit}	e (x_{fit}/x_0-1) (%)
δ_i	0.1	6	0.091	−9
δ_o	0.2	1/6	0.201	0.5
k_{12}^0	3	5	2.900	−3.3
k_{21}^0	4	1/5	3.807	−4.8
k_{34}	5	4	6.467	29.3
k_{43}	6	1/4	6.051	0.9
K_1^0	7	3	9.083	29.8
d_p	0.5	1/3	0.504	0.8
k_{ia}^0	0.1	2	0.106	6.0
k_{ai}^0	0.2	1/2	0.203	1.5
d_{ia}	0.3	1.5	0.293	−2.3
d_{ai}	−0.4	1/1.5	−0.397	−0.8
σ	0.10	4.033	0.099	–

Visually, the fit in Fig. 7A looks perfect. Figure 7B and Table 3 (column e), however, show that the individual parameters are found with different accuracies. For instance, the location $d_p = 0.5$ of the energy barrier for charge translocation and $k_{43} = 6$ which determines I_{S+} have been found with an accuracy below 1%, although the scatter $\sigma_0 = 0.1$ was 2.5% of the entire y-scale. On the other hand, k_{34} and ${K_1}^0$ are both found with an accuracy of 30% only, and without a tendency to converge to a better accuracy with additional iterations (right half of Fig. 7B). This parallel deviation reflects the finding in Fig. 3 that ${K_1}^0$ (panel B) and k_{34} (panel M) can have very similar effects on $I_a(V)$. Altogether, Fig. 7 shows that the 12 parameters of the model can be identified with fair accuracy and low ambiguity from noisy current records from V-clamp experiments performed with a triangular V protocol.

In the present example, two $dI(V,t)$ recordings for $c_o = 1$ and 5 have been generated and analyzed. In principle, one $dI(V,t)$ may be sufficient for a fair determination (reconstruction) of the system parameters x_0. However, initial attempts to do so yielded no convincing results (data not shown); possibly very small initial dx and correspondingly very long computation times are necessary to obtain fits with $\sigma < \sigma_0$ from a single $dI(V,t)$ recording. It is recommended, therefore, to use several $dI(V,t)$ recordings with different $c_o > 0$, for reliable determination of the 12 system parameters.

Figure 8 shows that the fits which are based on the experimental $dI(V,t)$, do not only describe the experimental data fairly well (Fig. 7A) but lead to very good approximations of the individual functions $I_a(V)$ (Fig. 8A) and $p_a(V,t)$ (Fig. 8B), which act together in generating the final function $dI(V,t)$ via Eq. (1). The systematic deviations between original and fitted data, which cancel each other to yield the perfect fits with $\sigma < \sigma_0$ (Fig. 7A, Table 3, column d), are very small; apparently, there are no families but individual functions of $I_a(V)$ and $p_a(V,t)$ that account for the good fit by the product $I_a p_a$ in Eq. (1).

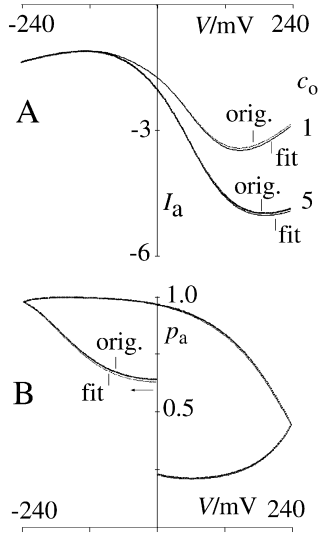

Fig. 8 "True" and inferred $I_a(V)$ (**A**) and $p_a(V,t)$ (**B**), plotted in $I_a(V)$ and $p_a(V)$ coordinates, respectively, as intermediate relationships for the fit in Fig. 7; curves fitted; dots (hardly visible) "measured"

Discussion

The results show that the presented model with all its simplifications can describe a large variety of electrical properties of ion translocating processes. The question is, however, whether the model in its general form is adequate to describe the electrical properties of specific transporters, which are more complicated. Before this question will be answered with respect to transporters of known properties, some apparent restrictions of the model should be addressed.

Charge relations of the transporter

For the sake of simplicity, the charge relations of the transporter have been treated here in a very crude way by discriminating only the two model versions MV1 and MV2. In reality, the charge relationships between transporter and ion are much more complicated and comprise multiple sites, resulting in non-integer effects on the translocated ion. In principle, these relationships might be treated by an extension of the presented model, in which the apparent charge z_b of the binding site varies not only between 0 and −1, but can assume any rational number. The considerable differences between the two model versions MV1 and MV2, presented here, indicate that the additional system parameter z_b could be fitted as well.

Temporal resolution of the enzymatic cycle

Another simplification of our model is to assume that the enzymatic transport cycle is fast compared with the recording cycle. This assumption is realistic with respect to previous applications of the triangular V clamp (Gradmann and Boyd 1999; Boyd et al. 2003) in the range of a second, compared with usual turnover numbers of ion transporters in the range of 100 s^{-1} and higher. As long as this steady-state assumption holds, the results about the enzymatic cycle will not depend on the recording speed, and we cannot say whether we are investigating many slow transporters or a few fast ones. This question would be answered, however, if the measuring velocity became approximately as fast as the transport cycle. In this case the apparent kinetic properties of the transport cycle will depend on the recording speed. Corresponding investigations of an ion pump have already been performed with fast sinusoidal V protocols (Tittor et al. 1983); they should be equally successful with fast triangular ones.

Fast binding/debinding

The assumption that the translocation steps are slow compared with the binding/debinding reactions (k_{12}, k_{21}, k_{34}, $k_{43} << k_{13}$, k_{31}, k_{24}, k_{42} in Fig. 1A) leads to the convenient introduction of the stability constants K_1 and K_2. The inverse proportionalities of I_S and K in Eq. (14) allow one to read from I_S versus $1/c$ plots whether the assumption of fast binding and debinding holds. Let us focus on I_{S+} for a moment. If we operate at high c_i, to ensure $k_{31} = k_{31}{}^0 c_i >> 1$, I_{S+} will cease its proportional rise with $1/c_o$ through $k_{42} = k_{42}{}^0 c_i$ in $K_2 = k_{42}/k_{24}$ when $k_{42} = k_{42}{}^0 c_i$ becomes comparably small as k_{43}. In fact, for very small c_o, I_{S+} will reach a maximum of k_{24}. Gradmann et al. (1987) have presented algebraic details and practical instructions for determining all eight rate constants of the four-state model from steady-state $I(V)$ relationships at various c_i and c_o, in cases when the assumption of fast binding/debinding does not apply.

More complicated gating schemes

The two-state gating scheme used here is also a severe simplification, a first approach. Reaction schemes with many more states and non-integer, rational numbers of apparent gating charges are necessary to describe the observed details of V-gating of ion channels appropriately (Zagotta et al. 1994; Jiang et al. 2003). In principle, gating models having more states and reaction steps with specific V sensitivities can also be assessed and analyzed by V-clamp experiments with triangular V protocols (Gradmann and Boyd 1999; Boyd et al. 2003). However, the resolution with the fast triangular V protocol is not as good as the resolution with conventional but time-consuming V-step routines, with step durations, which allow even the slowest relaxation process to come to an apparent rest.

Channels

The velocity of a triangular V-clamp has been used to resolve the gating properties of K^+ and Cl^- conductances (probably channels) during electrical excitations in the marine diatom *Coscinodiscus wailesii* (Gradmann and Boyd 2000), which takes place in the temporal range of a second.

It is popular to distinguish channels as high turnover uniporters from low throughput carriers, whereby the kinetics of carriers are usually assigned to reaction schemes with conformational changes such as the four-state model in the center of Fig. 1A, and channels are assigned to pores with a rigid structure even in the selectivity filter. The latter aspect is supported by "...absence of any significant activation free energy barrier..." for K^+ conduction through K^+ channels (Bernèche and Roux 2001), which is meant relative to diffusion. In absolute terms, however, the movement of K^+ through the selectivity filter does carry out a well-defined reaction cycle with a series of correspondingly small and flexible energy barriers (Bernèche and Roux 2001; Morais-Cabral et al. 2001). This can be presented in a simplified four-state model (fig. 5 in Morais-Cabral et al. 2001) similar to the one in Fig. 1A here. Are these barriers really insignificant for the electrophysiologist? They correspond to high conduction near the limits of diffusion (Bernèche and Roux 2001; Morais-Cabral et al. 2001), and may be detected electrophysiologically if saturation currents at $V << 0$ or $V >> 0$ are investigated. In case of strict diffusion limitation, these currents must be proportional to the substrate concentration c_S in the source compartment. If these saturation currents rise less than proportionally with c_S, limitation by the enzymatic reaction cycle (v_{max} in traditional Michaelis–Menten kinetics) of the selectivity is likely to take place.

Electrophysiological data from animal cells and artificial membranes are usually restricted to a rather narrow V range, so V saturation of membrane currents is mostly out of experimental reach in these systems. From plant membranes, however, which can be investigated over a much wider V range, enzymatic V saturation of currents through active K^+ channels has been reported (Gradmann et al. 1987; Klieber and Gradmann 1993).

Ion pumps

Hansen et al. (1981) have presented an approach for the reaction kinetic treatment of steady-state $I(V)$ curves of electrogenic ion pumps. The central reaction scheme in their study is the cyclic four-state model for ion transport (Läuger 1980), which is frequently under-rated as a "carrier" model, but is used here again (Fig. 1A) in its original and general meaning. Interestingly, triangular V-clamp experiments on marine diatoms have revealed V-gating (including its kinetic characteristics) of an electrogenic ion pump (Gradmann and Boyd 2000).

Cotransporters

Cotransport is accomplished by several families of proteins, such as the monomeric proteins of the major facilitator superfamily (MFS) with generally 12 membrane-spanning helices. The lactose permease of *E. coli* is maybe its biochemically best analyzed member, with a detailed reaction scheme of its operation derived from its 3D structure (Abramson et al. 2003). This reaction scheme corresponds to that in Fig. 1A when the (fast) serial binding/debinding steps of the two substrates (H^+ and S) inside and outside are lumped as corresponding equilibrium constants K_1 and K_2, and the actual translocation steps reflect crucial conformational changes. The most detailed application of the methods presented here has recently been worked out for the kinetic characterization of another MFS protein, the $2H^+$-

NO_3^-symporter from the fungus *Emericella nidulans* (Boyd et al. 2003). In this experimental investigation, the theory for the applied analysis was kept very short, prompting us to present a deeper and more general, theoretical background of the corresponding methods in more detail by this study.

Acknowledgements This work has been supported by grants from the Natural Sciences and Engineering Research Council of Canada to C.M.B.

References

Abramson J, Smirnova I, Kasho V, Verner G, Kaback HR, Iwata S (2003) Structure and mechanism of the lactose permease of *Escherichia coli*. Science 301:610–615

Bernèche S, Roux B (2001) Energetics of ion conduction through the K^+ channel. Nature 414:73–76

Boyd J, Gradmann D, Boyd CM (2003) Transinhibition and voltage-gating in a fungal nitrate transporter. J Membr Biol 195:1–12

Eisenberg RS (1990) Channels as enzymes. J Membr Biol 115:1–12

Fingerle J, Gradmann D (1982) Electrical properties of the plasma membrane of microplasmodia of *Physarum polycephalum*. J Membr Biol 68:67–77

Gradmann D, Boyd CM (1999) Electrophysiology of the marine diatom *Coscinodiscus wailesii* IV: types of non-linear current-voltage-time relationships recorded with single saw-tooth voltage-clamp. Eur Biophys J 28:591–599

Gradmann D, Boyd CM (2000) Three types of membrane excitations in the marine diatom *Coscinodiscus wailesii*. J Membr Biol 175:149–160

Gradmann D, Klieber H-G, Hansen U-P (1987) Reaction kinetic parameters for ion transport from steady-state current-voltage curves. Biophys J 51:569–585

Gradmann D, Johannes E, Hansen U-P (1997) Kinetic analysis of Ca^{2+}/K^+ selectivity of an ion channel by single-binding-site models. J Membr Biol 159:169–178

Hansen U-P, Gradmann D, Sanders D, Slayman CL (1981) Interpretation of current-voltage relationships for "active" ion transport systems. I. Steady-state reaction-kinetic analysis of Class-I mechanisms. J Membr Biol 63:165–190

Hille B (1984) Inonic Channels of Excitable Membranes. Sinauer Associates Inc., Sunderland, Massachusetts, p 187

Hookes R, Jeeves T (1961) "Direct Search" solution of numerical and statistical problems. J Assoc Comput Mach 8:212–229

Jiang Y, Ruta V, Chen J, Lee A, MacKinnon R (2003) The principle of gating charge movement in a voltage-dependent K^+ channel. Nature 423:42–48

Junge W, Lill H, Engelbrecht S (1997) ATP synthase: an electrochemical transducer with rotatory mechanics. Trends Biochem Sci 22:420–423

Kinraide T (2001) Ion fluxes considered in terms of membrane-surface electrical potentials. Aust J Plant Physiol 28:605–616

Klieber HG, Gradmann D (1993) Enzyme kinetics of the prime K^+ channel in the tonoplast of *Chara*: selectivity and inhibition. J Membr Biol 132:253–265

Läuger P (1980) Kinetic properties of ion carriers and channels. J Membr Biol 57:63–178

Läuger P (1995) Conformational transitions of ionic channels. In: Sakmann B, Neher E (eds) Single-channel recording, 2nd edn. Plenum, New York, pp 651–662

Maathuis FJM, Sanders D, Gradmann D (1997) Kinetics of high affinity K^+ uptake in plants, derived from K^+-induced changes in current-voltage relationships. Planta 203:229–236

Morais-Cabral J, Zhou Y, MacKinnon R (2001) Energetic optimization of ion conduction rate by the K^+selectivity filter. Nature 414:37–42

Neher E, Stevens CF (1977) Conductance fluctuations and ionic pores in membranes. Annu Rev Biophys Bioeng 6:345–381

Tittor J, Hansen U-P, Gradmann D (1983) Impedance of the electrogenic Cl^- pump in *Acetabularia*: electrical frequency entrainments, voltage-sensitivity and reaction kinetic interpretation. J Membr Biol 75:129–139

Zagotta WN, Hoshi T, Aldrich RW (1994) Shaker potassium channel gating. III. Evaluation of kinetic models for activation. J Gen Physiol 102:321–362